Ultrafine three-dimensional nanostructuring in YAG via seed-enabled femtosecond-laser near-field enhancement and wet etching

SUPPLEMENTARY INFORMATION

Jie Wu[1], Sikun Zhou[2, 3], Jing Li[1], Yangliu Zhai[1], Fangjie Wang[1], Han Qi[1], Rubo Chen[1], Hao Zhou[1], Shutong Wang[1], Guoliang Deng[1, *], Shouhuan Zhou[1]

1 College of Electronics and Information Engineering, Sichuan University, Chengdu 610064, China

2 Institute of Applied Electronics, CAEP, Mianyang, Sichuan 621900, China

3 National Key Laboratory of Science and Technology on Advanced Laser and High Power Microwave, Mianyang, Sichuan 621900, China

* gdeng@scu.edu.cn

Table of Contents

Supplementary Note 1. Material-property changes calculated using the Drude model

When materials are irradiated by laser, the density of free charge carriers within the material changes. According to the Drude model[1, 2], a change in the free charge carrier density causes a change in the material's dielectric constant ε. The calculation formula is:

$$\varepsilon = 1 + (\varepsilon_{\text{initial}} - 1)\left(1 - \frac{N_e}{N_0}\right) - \frac{\omega_p^2}{\omega^2\left(1 + i\frac{\nu_e}{\omega}\right)}$$

Here, $\varepsilon_{\text{initial}}$ denotes the dielectric constant of the material in its initial state, N_e represents the carrier density within the material, N_0 indicates the initial number of electrons in the valence band, and ω_p signifies the plasma frequency. The value of ω_p is calculated as $\omega_p = \sqrt{N_e e^2/\left(m^*_{\text{opt}}\varepsilon_0\right)}$ where e is the elementary charge, m^*_{opt} is the optical effective mass, ε_0 is the vacuum permittivity, ω is the angular frequency of the incident laser, and ν_e is the carrier collision frequency. This paper calculates the dielectric constant of the material at various carrier densities using the following formula. The near-field energy distribution is computed via simulation models to compare the electric field strength with and without the seed.

Supplementary Note 2. The effect of seeds on material absorption

To test the effect of modified seeds on material transmittance, we designed an in-situ experiment with the optical setup shown in Fig. S1a. The incident laser beam was split into two paths: one directed to detector 1 to monitor the laser output intensity, while the other was focused into the sample, then collected by an objective lens and incident to detector 2. During the experiment, the material was first modified internally using the processing laser. Subsequently, the laser frequency was reduced to 1 kHz, and the relative transmittance at different laser powers was measured with and without modified seeds, as shown in Fig. S1b. The results show that transmittance in the presence of seeds is consistently lower than that without seeds. The decrease in material transmittance may be influenced by two factors: scattering introduced by the seeds and enhanced absorption by the modified seeds.

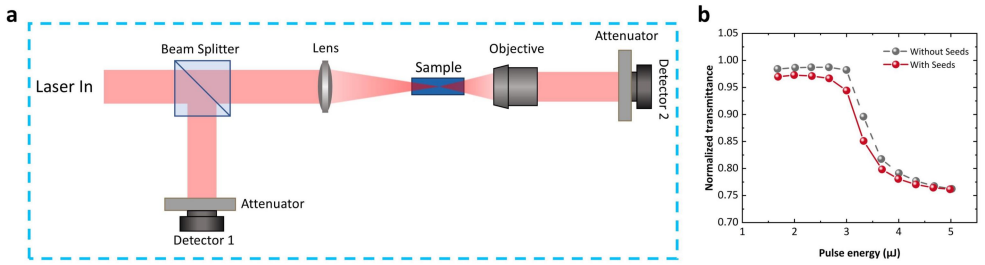

Figure S1: In-situ detection experiment. a, the optical path diagram of the in-situ detection experiment. **b**, the measured transmittance curve.

Supplementary Note 3. Laser processing chracteristics with seed-assisted modification under low NA (0.42) objectives

The first step of femtosecond laser enhanced wet etching is material modification by the laser. Because the modified regions produced with an oil-immersion objective are located inside the material and range from several tens to ~200 nm in size, they cannot be directly observed with optical microscopy or similar techniques. To investigate the properties of femtosecond laser processing based on the internal seeds, we conducted systematic experiments using a high-magnification objective (50×), so that the results could guide nanoscale structuring with the oil-immersion objective. Since neither the laser power nor the morphology of seed structures significantly influence the subsequent processing threshold, all seed structures were simplified to linear modifications inscribed inside the crystal, and all subsequent scans were initiated from these lines. We systematically compared, with and without seeds, the effects of different laser powers and scan speeds on the resulting structures (Fig. S2). Figure S2a shows how scan speed affects the modification results when seed structures are present (each condition repeated three times). At a scan speed of 0.05 mm/s, a continuous modification line could not be formed. As the speed increases, the modified length decreases further, and becomes nearly zero at 0.5 mm/s. These results indicate that femtosecond laser processing based on internal seeds is suitable at low scan speeds. Figure S2b compares the modification thresholds with and without seeds at different scan speeds, where the threshold is defined as the minimum laser power required to stably inscribe a modification line longer than 1 mm in the material. At higher scan speeds (>0.5 mm/s), thresholds were nearly identical for both cases. As the speed decreased, the threshold without seeds gradually decreased and stabilized around 60 mW at speeds below 0.1 mm/s. In contrast, with seeds the threshold reduction was more pronounced and consistently lower, reaching ~48 mW at 0.025 mm/s. These results demonstrate that femtosecond laser processing with internal seeds is strongly influenced by the incubation effect: under multi-pulse irradiation, the

modification threshold decreases significantly as the number of pulses increases. Therefore, lower scan speeds facilitate lower modification thresholds, and all subsequent experiments were performed at a scan speed of 0.01 mm/s.

Figure S2c shows the top- and side-view images of structures fabricated with and without seeds under the same scan speeds and processing depths. Without seeds, the femtosecond laser modification threshold is 60 mW, whereas with seeds it decreases to 48 mW. Thus, the introduction of seeds reduces the modification threshold to ~80% of its original value when using the 50× objective. The side-view images further reveal that the structural dimensions gradually shrink as the laser power decreases. Figure S2d presents the relationship between laser power and structural dimensions, with and without seeds, at the same scan speed of 0.01 mm/s. When seeds are present, the threshold is markedly lower, and both the width and height of the structures gradually diminish as the power decreases. These results demonstrate that in seed-assisted internal processing, lower scan speeds facilitate lower modification thresholds, and the corresponding lower laser power enables the fabrication of smaller-scale structures.

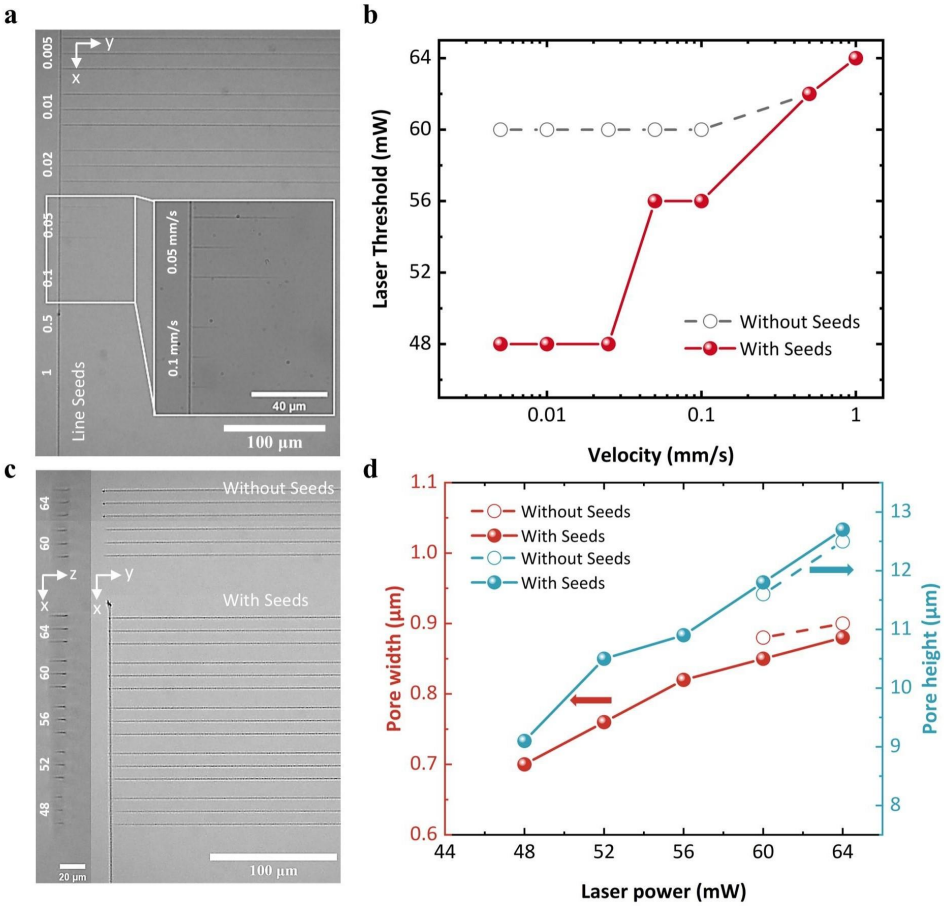

Figure S2 | Seed-assisted femtosecond laser processing under a low-NA (0.42) objective. **a**, optical microscope images of f seed-assisted processing at different scan speeds under the same laser power. The numbers indicate the scan speeds (mm/s). **b**, variation of the

modification threshold with scan speed under otherwise identical conditions. **c**, optical microscope images of line scans performed with and without seeds at different laser powers under otherwise identical conditions. The numbers indicate the laser power (mW). **d**, dependence of the line-scan structural dimensions on laser power with and without seeds.

Supplementary Note 4. Effect of laser polarization on the threshold of seed-assisted femtosecond laser processing

To investigate the influence of laser polarization on the threshold reduction observed in femtosecond laser processing based on the internal seeds, we examined the modification thresholds with and without seeds using objectives of different magnifications, as shown in Fig. S3a and S3b. The results show no significant difference between the two polarizations, regardless of the presence of seeds. This finding indicates that curved structures can be fabricated without changing the polarization during processing. As demonstrated in Fig. S3c, we fabricated a five-ring structure under sub-threshold conditions without altering polarization.

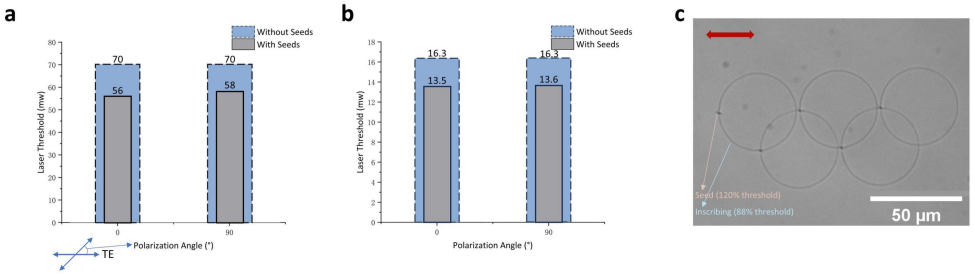

Figure S3 | Effect of polarization on seed-assisted femtosecond laser processing. a, Modification threshold variation with different polarizations, with and without seeds, using the 50× objective. **b**, Modification thresholds under different polarizations, with and without seeds, using the oil-immersion objective. **c**, Five-ring structure fabricated under sub-threshold condition with linear polarization.

Supplementary Note 5. Evolution of structural morphology and supercontinuum spot patterns at different stages

To examine how structural morphology evolves with decreasing laser power, we compiled cross-sectional images of structures at different stages together with the

corresponding supercontinuum spot patterns recorded by the CMOS camera, as shown in Fig. S4. As shown in Figs. S4a and S4b, structures fabricated with both linearly and circularly polarized light exhibit three characteristic morphological stages. While the morphological features of each structural stage remain unchanged as power decreases, the overall structural dimensions are significantly reduced. Figs. S4c and S4d highlight the contrasting evolution of supercontinuum spots with and without seeds: with seeds, the spot decreases gradually with power, whereas without seeds it decreases abruptly.

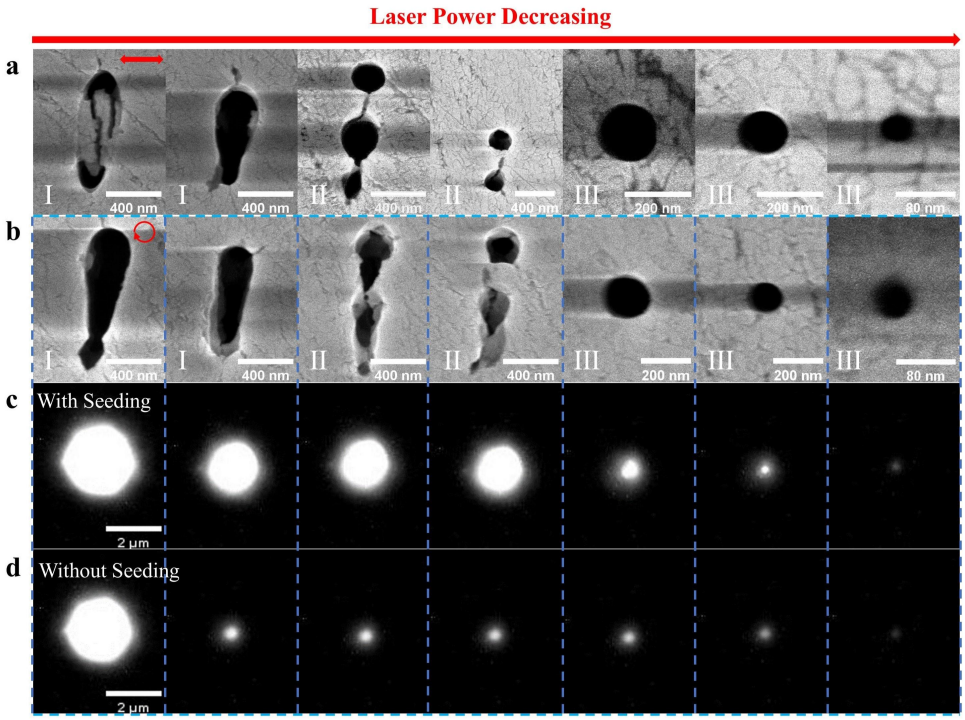

Figure S4 | Structures evolution and corresponding supercontinuum spot patterns in seed-assisted femtosecond laser processing. a, SEM images of structures fabricated at different powers with linearly polarized light with internal seeds. **b**, SEM images of structures fabricated at different powers with circularly polarized light with internal seeds. (**c**, **d**) Real-time supercontinuum spot patterns observed by the CMOS camera during the processing of the structures shown in (b), with seeds (c) and without seeds (d), respectively. A common scale bar is shared between (c) and (d).

Supplementary Note 6. Effect of etching time on the cross-sectional morphology of nanopores

Because the fabrication of nanopores requires wet etching, the duration of

etching has a pronounced effect on the resulting structures. Structural changes under different etching times are shown in Fig. S5. Figures S5a and S5b compare structures of various sizes fabricated with linearly and circularly polarized light, respectively, as a function of etching time. Within the first 4 h, the structural dimensions show no significant change, although slight deformations appear in some pores. After 49 h of etching, however, all structures evolve into hexagonal geometries with markedly increased dimensions. Similar hexagonal morphologies have also been reported previously[3].

To obtain small through-holes, the etching time is preferably limited to less than 4 h, which can be achieved by introducing auxiliary vertical etching pores[4, 5]. Nevertheless, the successful fabrication of nanopores and photonic crystal structures composed of through-holes also requires a high-precision translation stage and a stable experimental environment.

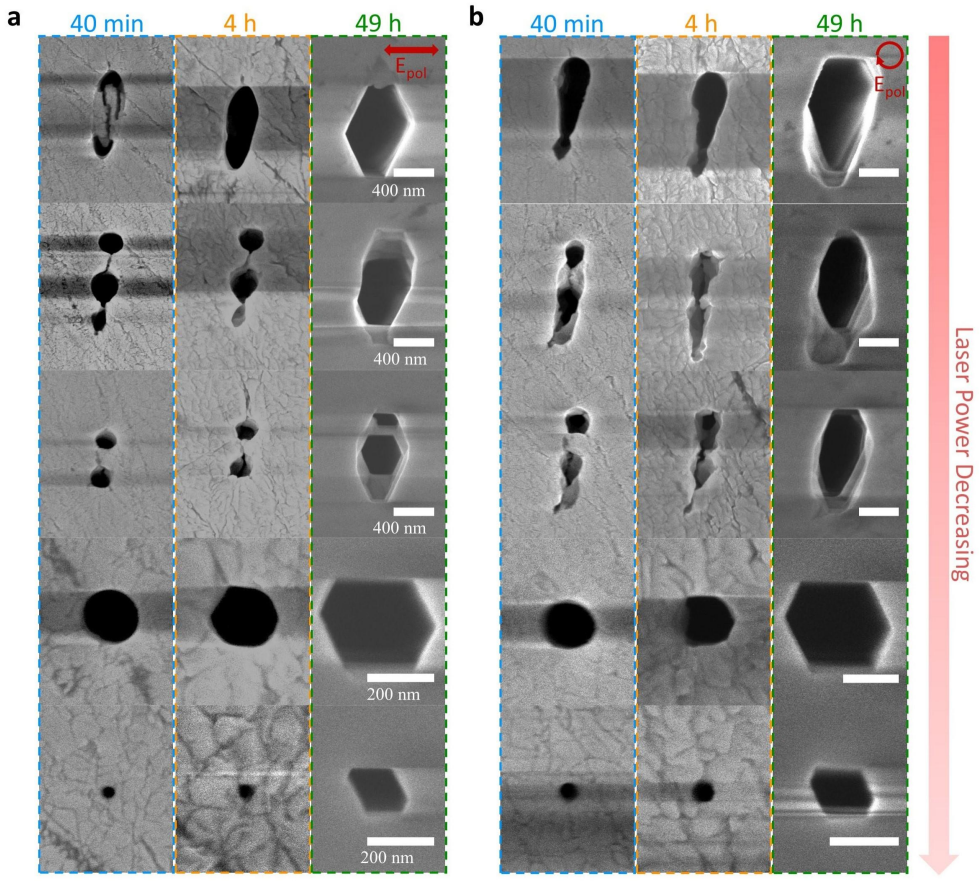

Figure S5 | Effect of etching time on nanopores morphology. a, evolution of nanostructures of different sizes with etching time under linear polarization. **b**, evolution of nanostructures of different sizes with etching time under circular polarization.

Supplementary Note 7. Applicability of seed-assisted femtosecond laser processing in sapphire

The seed-assisted femtosecond laser processing proposed in this work is also applicable to sapphire, as demonstrated in Fig. S6. In sapphire, the modification threshold is about 149 mW without seeds, whereas with seeds it decreases to 91 mW, corresponding to ~60% of the original threshold.

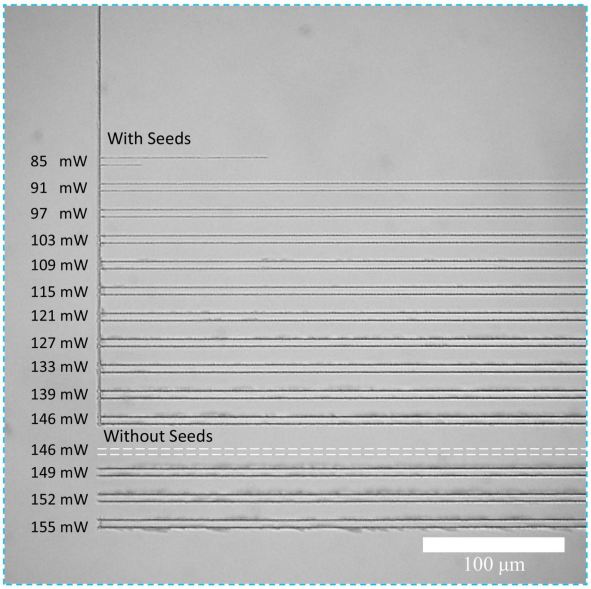

Figure S6 | Applicability of seed-assisted femtosecond laser processing in sapphire

Supplementary Note 8. Discussion on the influence of initial seeds and other conditions on the fabrication of seed-based photonic crystal structure waveguides

Given that our method requires the fabrication of an initial seed, whose presence can influence both the final processed structures and the etching dynamics, we discuss here several potential effects arising from this requirement.

(1) For the requirements and geometrical limitations in terms of proximity of the seeds, we propose two processing strategies to mitigate their influence.

First, in applications such as photonic-crystal waveguides where the seed region is not functionally required, the portion containing the initial seed can be removed by

post-processing grinding and polishing. This approach eliminates the seed's influence on the final architecture, though it results in a shorter overall structure—a trade-off we find acceptable for certain designs.

Alternatively, seeds can be fabricated outside the target structure to avoid embedding them within functional regions. As shown in Fig. S7, a seed is first written outside the intended pattern. The laser beam is then scanned in the X-direction from the seed to the starting point of the structure using power below the intrinsic modification threshold (i.e., the threshold without seeds). Finally, the entire structure is fabricated by scanning in the Y-direction. Because the threshold reduction enabled by the seed is largely independent of laser polarization, the transition from X-directional to Y-directional scanning introduces negligible processing artifacts. The modified traces generated along the X-direction can also function as auxiliary etching channels. To fully etch the structure, only subsequent vertical (Z-direction) auxiliary etching lines need to be fabricated.

(2) For the length of the structure that can be fabricated, nanopores up to approximately 100 μm can be produced while maintaining structural size and roundness, without employing auxiliary vertical etching. If such auxiliary vertical etching channels are incorporated, the feasible pore length can, in principle, be extended without limit. Aligning these auxiliary features precisely continues to be difficult because of environmental fluctuations, limited translation-stage accuracy, and laser-power instability. We plan to tackle these alignment challenges in future studies.

(3) In this paper, we focus on demonstrating the fabrication of near-circular-sized tailorable nanopores down to several tens of nanometers with seed-enabled femtosecond-laser near-field enhancement and wet etching. The optimal etchant for nanostructures fabricated via seed-assisted femtosecond laser writing may differ from that used for conventional seedless structures, owing to differences in chemical accessibility and modified-region morphology. Understanding these etching requirements is crucial for reliably producing nanoscale features. To the best of our knowledge, systematic studies correlating structural dimensions with etchant selection at nanoscale size and under seed-enabled processing conditions have not been reported. Etching mechanisms and optimization will be investigated in future work.

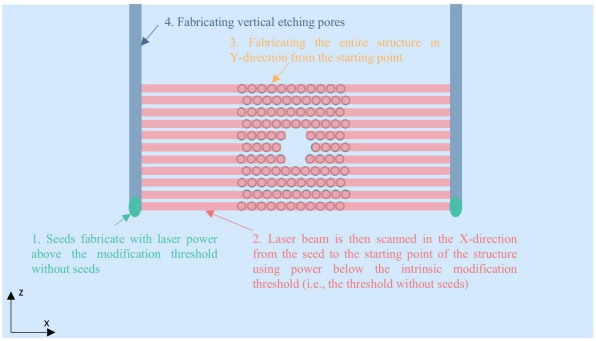

Figure S7 | Schematic diagram of the processing of the photonic crystal waveguide structure completed with the seeds outside the structure.

Supplementary Note 9. Effect of the seeds writing power and the size of the seeds on the threshold of seed-assisted femtosecond laser processing

We investigated how the modification threshold depends on the laser power used to fabricate the initial seeds, as this parameter determines the seed size. Fig. S8a shows optical micrographs of line scans performed near the seeded modification threshold using different seed-writing powers. Under varying initial seed conditions created by different laser powers, processing was performed using three sets of laser-power steps (3 mW per step), with three lines fabricated per set. The dimensions of the seed structures (in the xz-plane) vary with the seed-writing laser power. Across the tested power range, a continuous line is fabricated only at 58 mW, whereas lower powers fail to produce a complete line. Fig. S8b summarizes how the seeded modification threshold varies with seed-writing power. The results indicate that the modification threshold in the presence of seeds remains largely constant, independent of both the seed-writing power and the resulting seed size.

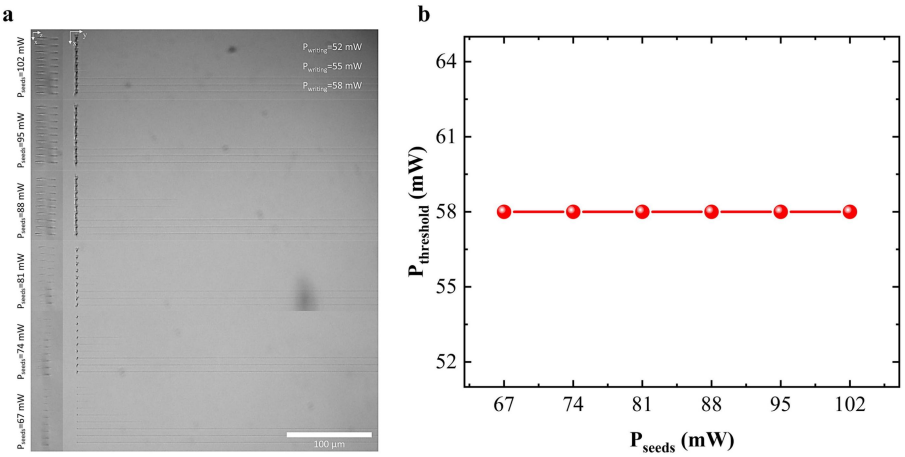

Figure S8 | Effect of the seeds writing power and the size of the seeds on the threshold of seed-assisted femtosecond laser processing. a, optical microscope images of line scans performed with different seeds writing power near the threshold with seeds. **b**, variation of the modification threshold with seeds writing power under otherwise identical conditions.

Supplementary Note 10. Experiments on the repeatability and stability of nanopores

To evaluate the controllability and process stability of our proposed method over a range of feature sizes, we fabricated multiple nanopore arrays (five pores per array) at progressively lower laser powers. The resulting dimensions are summarized in Fig. S9a. The data show excellent repeatability for circular holes with diameters greater than 50 nm. As shown in Fig. S9b, our laser power stability currently hinders the reproducible fabrication of sub-50 nm nanopores. We anticipate that employing a laser source with superior power stability will not only enhance repeatability at the smallest achievable sizes but may also enable the fabrication of even finer nanostructures.

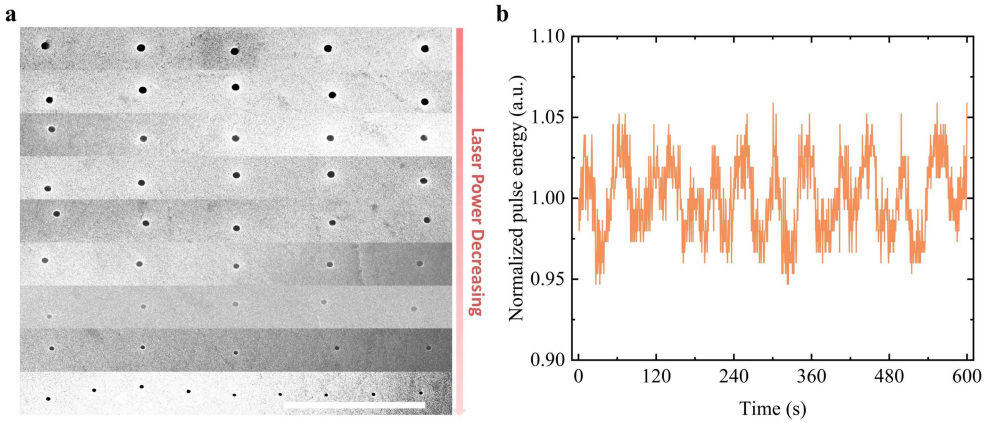

Figure S9 | Experiments on the repeatability and stability of nanopores. a, dot arrays as the laser power decreasing. The scale bar is 3 μm. **b**, The stability of laser pulse energy.

Reference

1. Bulgakova, N. M. et al. A general continuum approach to describe fast electronic transport in pulsed laser irradiated materials: The problem of coulomb explosion. *Applied Physics A* **81**, 345-356 (2005) doi: 10.1007/s00339-005-3242-0.
2. Sokolowski-Tinten, K. & von der Linde, D. Generation of dense electron-hole plasmas in silicon. *Physical Review B* **61**, 2643-2650 (2000) doi: 10.1103/PhysRevB.61.2643.
3. Okhrimchuk, A.G. et al. Inscription of a waveguide in yag:Nd crystal with a cladding composed by crystalline hollow channels. *Optical Materials Express* **12**, 1609-1616 (2022) doi: 10.1364/OME.447622.
4. Ródenas, A. et al. Three-dimensional femtosecond laser nanolithography of crystals. *Nature Photonics* **13**, 105-109 (2019) doi: 10.1038/s41566-018-0327-9.
5. WU, J. et al. Helical hollow channel waveguide in yag fabricated by femtosecond laser enhanced wet etching. *Optics Letters* **49**, 2441-2444 (2024) doi: 10.1364/OL.523400.